

## Durham Research Online

---

### Deposited in DRO:

31 May 2016

### Version of attached file:

Published Version

### Peer-review status of attached file:

Peer-reviewed

### Citation for published item:

Whitbourn, J.R. and Shanks, T. (2016) 'The galaxy luminosity function and the Local Hole.', *Monthly notices of the Royal Astronomical Society.*, 459 (1). pp. 496-507.

### Further information on publisher's website:

<http://dx.doi.org/10.1093/mnras/stw555>

### Publisher's copyright statement:

This article has been accepted for publication in *Monthly notices of the Royal Astronomical Society* ©: 2016 The Authors Published by Oxford University Press on behalf of the Royal Astronomical Society. All rights reserved.

### Additional information:

---

### Use policy

The full-text may be used and/or reproduced, and given to third parties in any format or medium, without prior permission or charge, for personal research or study, educational, or not-for-profit purposes provided that:

- a full bibliographic reference is made to the original source
- a [link](#) is made to the metadata record in DRO
- the full-text is not changed in any way

The full-text must not be sold in any format or medium without the formal permission of the copyright holders.

Please consult the [full DRO policy](#) for further details.

# The galaxy luminosity function and the Local Hole

J. R. Whitbourn<sup>★</sup> and T. Shanks<sup>★</sup>

*Extragalactic Astronomy Group, Department of Physics, Durham University, South Road, Durham DH1 3LE, UK*

Accepted 2016 March 4. Received 2016 February 9; in original form 2015 June 22

## ABSTRACT

In a previous study Whitbourn & Shanks have reported evidence for a local void underdense by  $\approx 15$  per cent extending to  $150\text{--}300\ h^{-1}$  Mpc around our position in the Southern Galactic Cap (SGC). Assuming a local luminosity function they modelled  $K$ - and  $r$ -limited number counts and redshift distributions in the 6dFGS/2MASS and SDSS redshift surveys and derived normalized  $n(z)$  ratios relative to the standard homogeneous cosmological model. Here we test further these results using maximum likelihood techniques that solve for the galaxy density distributions and the galaxy luminosity function simultaneously. We confirm the results from the previous analysis in terms of the number density distributions, indicating that our detection of the ‘Local Hole’ in the SGC is robust to the assumption of either our previous, or newly estimated, luminosity functions. However, there are discrepancies with previously published  $K$ - and  $r$ -band luminosity functions. In particular the  $r$ -band luminosity function has a steeper faint end slope than the  $r_{0.1}$  results of Blanton et al. but is consistent with the  $r_{0.1}$  results of Montero-Dorta & Prada and Loveday et al.

**Key words:** methods: analytical – galaxies: general – Local Group – large-scale structure of Universe – infrared: galaxies.

## 1 INTRODUCTION

Our local galaxy clustering environment has recently assumed even greater importance with the discovery that the SNIa *Hubble* diagram can be fitted by a Universe with an accelerating expansion rate (Schmidt et al. 1998; Perlmutter et al. 1999). Given the finely tuned nature of the vacuum energy that is implied by cosmological explanations of the form of the *Hubble* diagram (Carroll 2001), there is clear motivation to look for other explanations for this observation. This has led to a variety of activity investigating whether the local expansion rate is faster than at larger distances due to the presence of a Local Hole or Void. Indeed, there have been claims of a local underdensity manifesting as a local rise in SNIa-based measurements of  $H_0$  (Zehavi et al. 1998; Jha, Riess & Kirshner 2007). Although some authors attribute these results to systematics associated with dust (Conley et al. 2007), these results are consistent with other work where bulk flows out to  $z < 0.06$  are found using SNIa (Feindt et al. 2013; Colin et al. 2011; Wojtak et al. 2014) and the tension between local and CMB determinations of  $H_0$  (Planck Collaboration XVI 2014). Some of the work in this regard has even focused on non-Copernican models with the Local Group positioned at the centre of a large void (Clarkson & Maartens 2010; Schwarz 2012; Krasinski 2014). Here we are investigating a simpler scenario where the Local Group is at the edge of an underdense region that covers much of the Southern Galactic Cap (SGC). Evidence for

such a possibility has been presented by Shanks (1990), Zucca et al. (1997), Metcalfe et al. (2001, 2006), Busswell et al. (2004) and Frith et al. (2003), Frith, Outram & Shanks (2005), Frith, Shanks & Outram (2005) and Frith, Outram & Shanks (2006).

Whitbourn & Shanks (2014, the companion study to this paper, which we will refer to hereafter as [Paper I](#)), have also recently presented evidence for a local void with an  $\approx 15$  per cent underdensity out to  $\approx 150\text{--}300\ h^{-1}$  Mpc. These authors used 6dFGS/2MASS and SDSS redshift surveys to probe the local region by modelling the  $n(z)$  distributions from three large regions of sky covered by these surveys. They also used the  $\bar{z}(m)$  technique of Soneira (1979) to make a *Hubble* diagram based on the redshift survey galaxies and showed that the data preferred a model that showed coherent bulk motion out to  $150\ h^{-1}$  Mpc compared to a model where the galaxy motions recovered the CMB dipole within the survey region.

More recently Keenan et al. (2010, 2012) and Keenan, Barger & Cowie (2013) have compared galaxy counts and luminosity density at high and low redshift and reported evidence for a 300 Mpc void with a 50 per cent underdensity. Alternative probes than  $K$ -band galaxy surveys have also been used to study this hypothesis. In particular Böhringer et al. (2015) used the X-ray-selected REFLEX II cluster survey. These authors find evidence for significant underdensities with conclusions broadly similar to those of [Paper I](#).

In [Paper I](#) we traced the local  $n(z)$  using techniques that assumed the form of the luminosity function (LF) from previous work. The assumed form was also inferred in the  $r$  and  $K$  bands from original observations of LFs as a function of galaxy morphology/ $B - V$

<sup>★</sup> E-mail: [jrwhitbourn@gmail.com](mailto:jrwhitbourn@gmail.com) (JRW); [tom.shanks@durham.ac.uk](mailto:tom.shanks@durham.ac.uk) (TS)

colour in the  $B$  band. Here we return to the issue of the Local Hole now using maximum likelihood (ML) methods (Choloniewski 1987; Efstathiou, Ellis & Peterson 1988; Cole 2011) that solve for the galaxy density run with redshift,  $\phi(z)$ , simultaneously with solving non-parametrically for the LF. The only parameters needed are simple forms for the  $K$ -correction and evolution  $K + E$  terms.

In particular, we begin by describing the techniques used in estimating the galaxy LF and the underlying density fields. We first report the  $V/V_{\max}$  results for the  $K$  band and relate these results to the number count slopes reported in Paper I. We then show the  $K$ -band LFs and compare to the Metcalfe et al. (2001, 2006) LF assumed in determining the density profiles presented in Paper I. We proceed by presenting the density profiles estimated in conjunction with the LF's using ML methods. We also include similar results for the  $r$ -band SDSS sample.

Throughout this paper we use a flat  $\Lambda$  cold dark matter ( $\Omega_{\Lambda,0} = 0.7$ ,  $\Omega_{m,0} = 0.3$ ) cosmology with Hubble constant  $H = 100 h \text{ km s}^{-1} \text{ Mpc}^{-1}$  with  $h = 0.7$ .

## 2 TECHNIQUES

We now briefly describe the methods of estimating the galaxy LF used in this paper. Unless otherwise stated we have estimated non-parametric LFs using bin sizes of  $dM = 0.5$  and  $d\mu = 0.25$ .

### 2.1 Non-parametric luminosity function estimation

#### 2.1.1 $V_{\max}$ luminosity function

We have used the standard  $1/V_{\max}$  estimator (Kafka 1967; Schmidt 1968). This method assumes a homogeneous model and estimates the LF as

$$\phi(M) = \sum_i^N \frac{1}{V_{i,\max}} W(M_i - M), \quad (1)$$

where  $V_{\max}$  is the comoving volume associated with the maximum redshift this galaxy could be observed and  $W(M_i - M)$  is a window function describing the binning  $dM$  assumed for the LF, i.e.

$$W(M_i - M) = \begin{cases} 1 & \text{if } -dM/2 \leq (M_i - M) \leq dM/2 \\ 0 & \text{if else.} \end{cases} \quad (2)$$

One advantage of this method is the relative ease with which it can be extended to allow weighting of galaxies. This can be achieved by replacing the unity argument of the window function for galaxies in the absolute magnitude bin  $dM$  by a weighting factor (Ilbert et al. 2005). We have used the magnitude dependent completeness factor described in appendix II of Paper I, i.e.  $1/f(m_i)$  where  $f(m_i)$  is the spectroscopic success function described in Paper I. We can account for a bright magnitude limit by replacing  $V_{\max}$  by  $V_{\max} - V_{\min}$  in the denominator of equation (1) since this is now the volume over which the survey is complete at this absolute magnitude.

Whilst this estimator of the LF is minimum variance and ML it is also biased as it assumes homogeneity and will therefore be affected by LSS (Felten 1976). Importantly, other LF estimators are unaffected by LSS variations; hence, the difference between this LF estimator and the others is therefore reflective of the presence of LSS. Although this method offers an estimate of the global normalization of the LF, no estimate of the density run  $\phi(z)$  is available from this binned LF estimator.

#### 2.1.2 NPML: Choloniewski–Peebles luminosity function

An alternative approach is a non-parametric maximum likelihood (NPML) method due to PJE Peebles (private communication) and Choloniewski (1986). The NPML method assumes separable densities  $\rho_i$  and LF  $\phi_j$  with Poisson distribution in the brightness–distance modulus plane  $(M, \mu)$ . The probability for  $n_{i,j}$  galaxies to occupy the  $i, j$ th brightness–distance modulus bin is

$$p(N = n_{ij}) = \frac{\exp^{-\rho_i \phi_j} (\rho_i \phi_j)^{n_{ij}}}{n_{ij}!}. \quad (3)$$

Differentiating the log likelihood formed from these probabilities gives estimates that can be solved iteratively (Takeuchi, Yoshikawa & Ishii 2000):

$$\rho_i = \sum_j n_{ij} / \sum_j \phi_j \quad (4)$$

$$\phi_j = \sum_i n_{ij} / \sum_i \rho_i. \quad (5)$$

On the basis that the cross terms are zero, the Fisher matrix errors are simply

$$\sigma_{\rho_i} = \frac{\rho_i}{(\sum_j n_{ij})^{1/2}} \quad (6)$$

$$\sigma_{\phi_j} = \frac{\phi_j}{(\sum_i n_{ij})^{1/2}}. \quad (7)$$

This is a ML estimator method which is independent of inhomogeneity (Choloniewski 1986). Furthermore, it also offers an estimate of the global normalization of the LF and the density run  $\phi(z)$ . However the method's accuracy is dependent on galaxies being Poisson distributed across the brightness and distance modulus binning. The validity of this assumption is improved by smaller bin sizes but at the expense of possible bias (which increases with smaller bin sizes; Choloniewski 1986). We have used  $dM = 0.5$ ,  $d\mu = 0.25$  for the  $K$  band and  $dM = 0.2$ ,  $d\mu = 0.2$  for the  $r$  band.

#### 2.1.3 $C^-$ luminosity function

We have also used the  $C^-$  method of Lynden-Bell (1971) as updated by Choloniewski (1987). Here the distribution of galaxies in the  $(M, \mu)$  plane is used to infer a binned non-parametric LF.

For a sample sorted from brightest to faintest we construct the  $C^-$  statistic as (Lynden-Bell 1971) follows:

$$C^- = \sum_i^{M < M_i} \sum_{m_b - M_i \leq \mu_j}^{\mu_j \leq m_t - M_i} w_{ij}, \quad (8)$$

where  $w_{ij}$  is the weight of each galaxy which can be used to account for incompleteness (Ilbert et al. 2005). We have again accounted for incompleteness as  $w_{ij} = 1/f(m_{ij})$  where  $f(m_{ij})$  is the spectroscopic success function described in Paper I. The summation is defined by the ranges associated with the faint ( $m_t$ ) and bright ( $m_b$ ) magnitude limits.

These  $C^-$  coefficients can then be related to the cumulative LF  $\Phi(M)$  through a recursion relation. This method for estimating the cumulative LF was modified by Choloniewski (1987) who extended it to enable an estimate of the underlying LF with a global normalization and a density profile. It is this version of the estimator that we use in this study. Further discussion of the method can found in Choloniewski (1987), Willmer (1997) and Takeuchi et al. (2000).

### 2.1.4 Joint SWML method

The Efstathiou–Ellis–Peterson (EEP) estimator is a ML estimator which maximizes the probability of selection (Efstathiou et al. 1988):

$$p = \frac{\phi(M)}{\int_{M_b(z)}^{M_f(z)} \phi(M) dM}. \quad (9)$$

Here the bounds on the integral are defined by the selection criteria of the survey. We can therefore calculate the likelihood,  $\mathcal{L} = \prod_i^N p_i$ , over binned values of the LF to find the ML estimator. This binning of the LF requires the use of step-functions in describing the ML solution. This stepwise approach has led to the estimator being described as the Step-Wise ML (SWML) method. This method has been updated by Cole (2011) to jointly estimate the global normalization, density profiles and the LF (JSWML). It is this JSWML version of the NPML method that is used in this study.

Our implementation of this method is based on a modified version of the JSWML code provided by Cole (2011).<sup>1</sup> We have used the default settings except for implementing the K+E corrections described in Section 3.1, the specific cosmological parameters used in this paper and the absolute magnitude range required.

## 2.2 Parametric luminosity function estimation

The estimation of LFs can be analytically simplified by assuming a parametric form. This is typically achieved for galaxies by using a Schechter (1976) fit.

### 2.2.1 STY luminosity function

The Sandage–Tammann–Yahil (STY) method is akin to the EEP and JSWML methods in that it is a ML estimator (Sandage, Tammann & Yahil 1979). Here though we calculate the likelihood,  $\mathcal{L} = \prod_i^N p_i$ , over a plane of possible values of the Schechter parametrizations  $(\alpha, M_*)$  to find the ML estimates of the LF parameters.

We have evaluated  $\mathcal{L}(\alpha, M_*)$  over  $\alpha \in [0.8, 1.6]$  and have adapted the range for  $M_*$  for each sample on the basis of the estimated covariance matrix. In both cases we have used bin sizes of 0.01. Incompleteness effects can be accounted for by weighting each probability as  $p_i^{w_i}$  where  $w_i$  is the inverse of the spectroscopic success function  $f(m)$  described in Paper I. For a fuller discussion and a full expansion of the log likelihood, see Zucca, Pozzetti & Zamorani 1994 and Zucca et al. 1997. We note that this method estimates Schechter LF parameters  $(\alpha, M_*)$  but does not provide any estimate of the global normalization  $\phi_*$  or the density profile. It should also be noted that the accuracy of the STY LF estimates is dependent on the validity/accuracy of the assumed parametric form.

## 2.3 Luminosity function and density profile normalization

### 2.3.1 Luminosity function normalization

An LF normalization is related to the spatial number density as

$$n = \int_{-\infty}^{\infty} \phi(M) dM. \quad (10)$$

<sup>1</sup> These modifications resolved issues with the absolute magnitude bin centres and the number of redshift bins.

A minimum variance estimator ( $n_3$ ) was found by Davis & Huchra (1982) and has been commonly used. However, it is not an unbiased estimator for inhomogeneous samples as the number density is also present in the galaxy weighting. Although this effect is expected to be small (Willmer 1997; Keenan et al. 2012), we have decided to use an unbiased estimator of the number density (Davis & Huchra 1982):

$$n_1 = \frac{\int_0^{z_f} (N(z)/s(z)) dz}{\int_0^{z_f} dV}. \quad (11)$$

Here  $s(z)$  is the galaxy selection function and  $N(z)$  is the redshift distribution of galaxies. The disadvantage of this estimator is the instability associated with its heavier weighting of higher redshift objects where the selection function is more uncertain. Various methods such as using medians etc. have been proposed for improving the robustness of these estimators (de Lapparent, Geller & Huchra 1989). We consider a high-redshift cutoff of  $z_f = 0.04$  and  $z_f = 0.075$  in the estimation of  $n_1$  for the  $K$ - and  $r$ -band, respectively (i.e. approximately the maximum of the respective redshift distributions). The resulting unbiased estimator  $n_1$  can then be used to normalize  $\phi(M)$  following equation (10).

### 2.3.2 Density profile normalization

We have considered a variety of methods for normalizing the density profiles. In Willmer (1997) it was shown that a number count type estimator is relatively unbiased as compared to other ML estimates density estimates. These ML estimates showed an  $\approx 20$  per cent bias towards underestimating density. The results presented in this study are therefore based on a number count normalization derived for each respective LF estimate. The number count normalization has been made by estimating the change in  $\phi_*$  required to fit the number counts (as per the method in Efstathiou et al. 1988) and scaling the density profiles accordingly.

We have ensured that these number count based results are consistent with the  $n_1$  estimator used in normalizing the LFs by considering a number density profile estimator derived from the  $n_1$  estimator, i.e. the ratio of the expected number of galaxies in a redshift shell of thickness  $dz$  and the volume of the redshift shell:

$$\frac{n(z)}{n_1} = \frac{N(z)/s(z)}{\frac{dV}{dz} dz}. \quad (12)$$

The results obtained using the unbiased  $n_1$  estimator are in agreement with those shown, but with larger uncertainties. For further detail of the techniques we use in estimating the LF and its normalization, see Johnston (2011).

## 3 DATA AND MODELLING

The imaging and redshift surveys used here are the same as those used in Paper I, namely 2MASS (Jarrett et al. 2003) and SDSS (York et al. 2000) for near-infrared (NIR) and optical imaging and 6dFGS (Jones et al. 2004) and SDSS for  $K$  and  $r$  limited galaxy redshift surveys. We again adopt the Vega photometric system and use the Local Group rest frame whilst adopting the transformations outlined in Paper I. We also reprise the magnitude estimators used in Paper I, i.e. a scale error corrected form of the ‘ $k_{m\_ext}$ ’ magnitude for 2MASS objects and the ‘ $cmodel$ ’ magnitude for SDSS objects – see Paper I for further discussion. To minimize the effects of incompleteness for the  $r$ -band sample, we have employed the more conservative magnitude selection  $10 < r < 17$  than was used in

**Paper I.** We have used an expanded  $7.5 < K < 12.5$  selection criteria for the  $K$  band. We now use a  $7.5 < K$  bright limit rather than the  $10 < K$  used in **Paper I** in order to maximize sample completeness whilst avoiding the range affected by 2MASS deblending issues.

We have used a faint absolute magnitude limit of  $M - 5 \log h \leq -18$  and  $M - 5 \log h \leq -15$  for the  $K$ - and  $r$ -band, respectively. We have ensured the accuracy of our modelling procedures by validating with respect to simulated data.

Within these surveys we again use the same large target fields as used in **Paper I** (see fig. 1 and table 3 of **Paper I**). These regions are chosen so as to be relatively similar in their dimensions, whilst being as large as their constituent surveys' geometry allows a coherent field to be. The largest fields possible were preferred since these should minimize cosmic variance (each represents  $\approx 1/15$  of the sky). These fields were also selected to represent regions of interest such as the CMB heliocentric dipole pointing and the Great Attractor whilst avoiding the galactic plane.

We will use galactic coordinates to define the fields as being northern or southern, and use the different surveys to further distinguish the two galactic northern fields i.e.: SDSS-NGC (Northern Galactic Cap), 6dFGS-NGC and 6dFGS-SGC.

### 3.1 K-corrections and evolution

We have followed **Paper I** in assuming simple representations of the Bruzual & Charlot (2003) K-correction plus evolution models as used by Metcalfe et al. to fit galaxy counts and colours to much higher redshifts than those discussed here.

For simplicity we have used a simple representation for the  $\tau = 2.5$  Gyr,  $x = 3$  and  $\tau = 9$  Gyr,  $x = 1.35$  K+E corrections for early-type and late-type galaxies in the  $K$  band. For both types there is little difference here between the K- and K+E corrections out to  $z \approx 0.3$ .

In the  $r$ -band there is a bigger difference between the K and the K+E corrections. We therefore use the average  $r$ -band K+E correction for early-type and spirals assuming the same Bruzual & Charlot (2003) models as for  $K$  above. Although there is a slight approximation here involved in taking an average K+E/K-correction at the  $z = 0.1$  limit of the range of interest the difference is only 0.05–0.06 mag.

### 3.2 Error calculation

To estimate random errors we use  $10^\circ \times 10^\circ$  subfields to calculate jackknife errors as used in **Paper I**. We found the number of subfields only weakly effect error estimates. The only exception to this is our use of Fisher matrix errors in the case of the NPML LF estimator.

## 4 LUMINOSITY FUNCTIONS

### 4.1 $V/V_{\max}$ histograms

Before studying the LF estimates we first probe the  $V/V_{\max}$  statistic. This is of particular interest because it is closely related to the  $1/V_{\max}$  LF estimator but is also dependent on the homogeneity of the sample – see Section 2.1.1. The  $V/V_{\max}$  statistic has been calculated using the  $7.5 < K < 12.5$  selection criteria, incompleteness correction and the K+E prescription outlined in Section 3.1. The homogeneous expectation is therefore that the samples are uniformly distributed over the volume probed and hence the mean  $V/V_{\max} = 0.5$ .

We now show in Figs 1–3 a histogram of this statistic for the  $K$ -band data over our three target regions with a binning of

$d(V/V_{\max}) = 0.1$ . We find for the 6dFGS-NGC, 6dFGS-SGC and SDSS-NGC regions, mean values of  $V/V_{\max}$  of  $(0.498 \pm 0.008)$ ,  $(0.523 \pm 0.007)$  and  $(0.522 \pm 0.005)$ , respectively. We conclude that in the 6dFGS-SGC and SDSS-NGC regions, the data is not consistent with a uniform distribution and is in fact increasing with  $V/V_{\max}$ . Given that incompleteness effects have been included in the calculation of  $V_{\max}$ , the significant excess above the homogeneous prediction in the 6dFGS-SGC and SDSS-NGC regions indicates that these samples are being preferentially distributed at higher redshifts. We therefore conclude that there is significant evidence for an inhomogeneity, and in particular a local underdensity, on the basis of the  $V/V_{\max}$  statistic alone.

We also note that the sloping of the  $V/V_{\max}$  statistic is closely related to the rising number counts of these samples as was observed in **Paper I**. Indeed it is the 6dFGS-SGC region which has the most pronounced sloping in  $V/V_{\max}$  and was the most underdense in **Paper I**. Clearly however determining the density profile and its run with redshift requires solving for the density profile. But first we now investigate whether the LF of these samples is consistent with those of the Metcalfe et al. (2001, 2006) LF assumed in determining the density profiles presented in **Paper I**.

### 4.2 K-band LF estimates

We next use the LF estimators described in Section 2 to estimate the  $K$ -band LF in our three regions. In Figs 4–6 we show these estimates for the 6dFGS-NGC, 6dFGS-SGC and SDSS-NGC regions, respectively. These LFs have been normalized using their respective estimate of  $n_1$ .

Treating these fields in turn, we begin with the 6dFGS-NGC field shown in Fig. 4. We first note that the LF estimators are in agreement with the Metcalfe et al. (2001, 2006) type dependent Schechter LF (green solid line) until the very bright end ( $< M_* - 2$ ). The Metcalfe et al. LF is an optical LF which is translated into the NIR using an assumed mean colour so this agreement was not to be taken for granted. We also note that the parametric Schechter function fits provided by the STY method is in agreement with the other non-parametric LF estimates over much of the range in absolute magnitude. However, for the very bright end ( $< M_* - 2$ ) the STY result is an underestimate with respect to the non-parametric estimates. We interpret this as suggesting that Schechter parametrization of the LF is accurate in the main but does not fully represent the abundance of very bright objects such as brightest cluster galaxies – a conclusion also reached by other authors (Jones et al. 2006).

For the 6dFGS-SGC region shown in Fig. 5 we see a similar set of estimates to those obtained in the 6dFGS-NGC region up until the faint end ( $< M_* + 2$ ). The Metcalfe et al. LF is a reasonable fit to all the estimators over all but the brightest and faintest magnitudes. Indeed, this time the parametric estimator, the STY method, agrees well with the non-parametric estimates except for  $< M_* - 2$  and  $< M_* + 2$ . We again assign this relative excess of faint objects and deficit of bright objects relative to the non-parametric fits as due to a limitation of this parametrization. We also note that the  $V_{\max}$  estimator is significantly different from the other estimates. We attribute this to the inhomogeneity reported in this field in **Paper I**. This is consistent with the elevated value of  $\langle V/V_{\max} \rangle = (0.523 \pm 0.007)$  in this region as discussed in Section 4.

Now in Fig. 6 we show the LF estimators for SDSS-NGC region. We draw similar conclusions to the previous 6dFGS-SGC region. In particular the  $V/V_{\max}$  LF estimate is again significantly different from the other estimators, especially at the faint end. We again



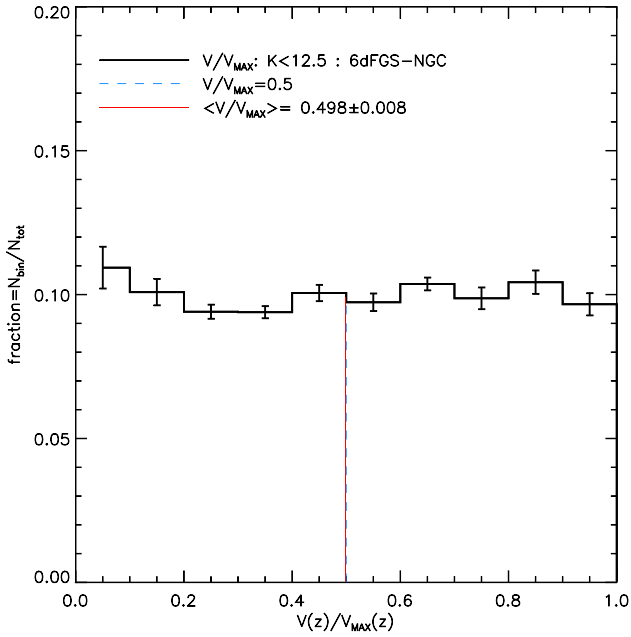


**Figure 1.** A histogram of  $K$ -band galaxy  $V/V_{\max}$  with  $7.5 < K < 12.5$  for the 6dFGS-NGC data with corresponding jackknife error. The blue (dashed) line shows the homogeneous expectation that  $\langle V/V_{\max} \rangle = 0.5$ . Also shown is the mean  $\langle V/V_{\max} \rangle$  for 6dFGS-NGC data (red, solid line).

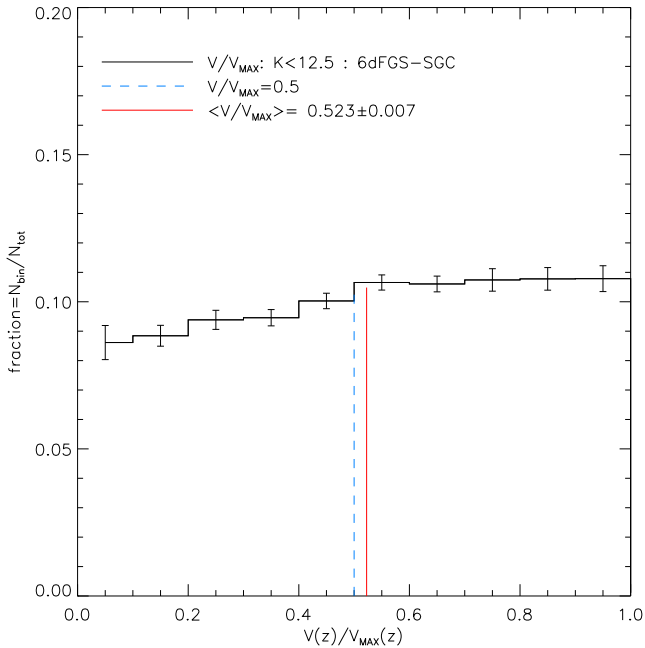


**Figure 2.** A histogram of  $K$ -band galaxy  $V/V_{\max}$  with  $7.5 < K < 12.5$  for the 6dFGS-SGC data with corresponding jackknife error. The blue (dashed) line shows the homogeneous expectation that  $\langle V/V_{\max} \rangle = 0.5$ . Also shown is the mean  $\langle V/V_{\max} \rangle$  for 6dFGS-SGC data (red, solid line).

attribute this to a significant inhomogeneity as indicated in this field by the elevated value of  $\langle V/V_{\max} \rangle = (0.522 \pm 0.005)$  discussed in Section 4. We also note that the bright end excess relative to the Schechter parametric fits is less pronounced in this field. We also observe that whilst the STY  $\alpha$  estimates are mutually consistent between the fields, the differences in the  $M_*$  estimates, although small, are significant. But in any case the differences are relatively

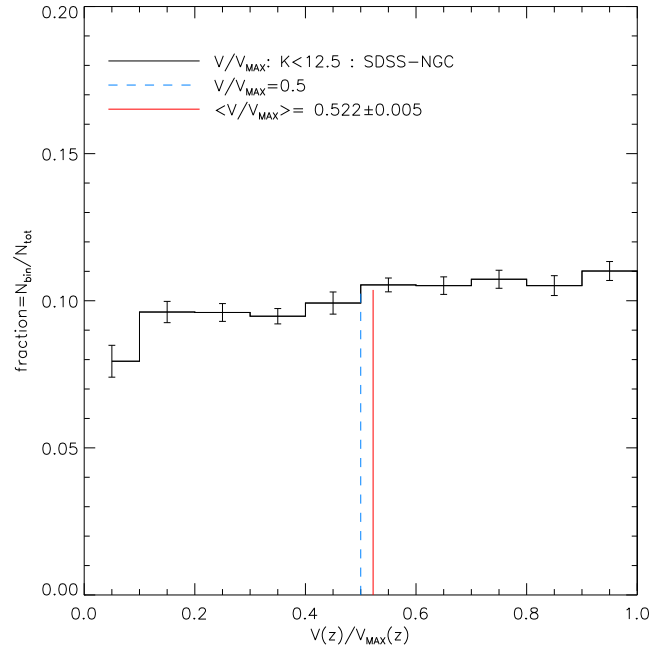


**Figure 3.** A histogram of  $K$ -band galaxy  $V/V_{\max}$  with  $7.5 < K < 12.5$  for the SDSS-NGC data with corresponding jackknife error. The blue (dashed) line shows the homogeneous expectation that  $\langle V/V_{\max} \rangle = 0.5$ . Also shown is the mean  $\langle V/V_{\max} \rangle$  for SDSS-NGC data (red, solid line).

minor in the sense that the Metcalfe et al. LF is a good representation of all the LF estimators except at the bright end.

We therefore conclude that the Metcalfe et al. LF is, for all three fields, an adequate fit to the majority of the  $K$ -band LF estimators. We take this as providing evidence supporting our assumption of the Metcalfe et al. LF in our previous study – [Paper I](#) – and hence the density profiles we then estimated using number counts. However, we can now continue this investigation beyond the LF and make use of the density profiles and normalization information provided by the various LF estimates to study the homogeneity of our samples.

## 5 $K$ -BAND NORMALIZED NUMBER DENSITY PROFILES

As outlined in Section 2 we can use the NPML, JSWML and  $C^-$  methods to estimate the run of the number density profile. The normalizations used are dependent on the estimator. The profiles presented here have been normalized using their respective LF-based number counts. Similar results, at greater uncertainty, are found when using the  $n_1$  unbiased number density estimator (i.e. equation 12) calculated using the corresponding LF. We now present in Figs 7–9 these number density profiles for the 6dFGS-NGC, 6dFGS-SGC and SDSS-NGC regions, respectively.

For the 6dFGS-NGC region (Fig. 7) we observe good consistency between the various estimates of the number density run. We can also see the inhomogeneity inferred from this field’s  $V/V_{\max}$  statistic in that locally ( $z < 0.05$ ) the profiles are typically underdense and then transition to being reasonably homogeneous. We also observe significant LSS clustering with significant fluctuations in the density profile at  $z \approx 0.048$  which we attribute to the Shapley-8 supercluster. We also note that this profile is similar to that presented in [Paper I](#) (fig. 3a) for the 6dFGS-NGC field where the Metcalfe et al. LF was assumed. This is in line with the agreement we noted in Section 4.2

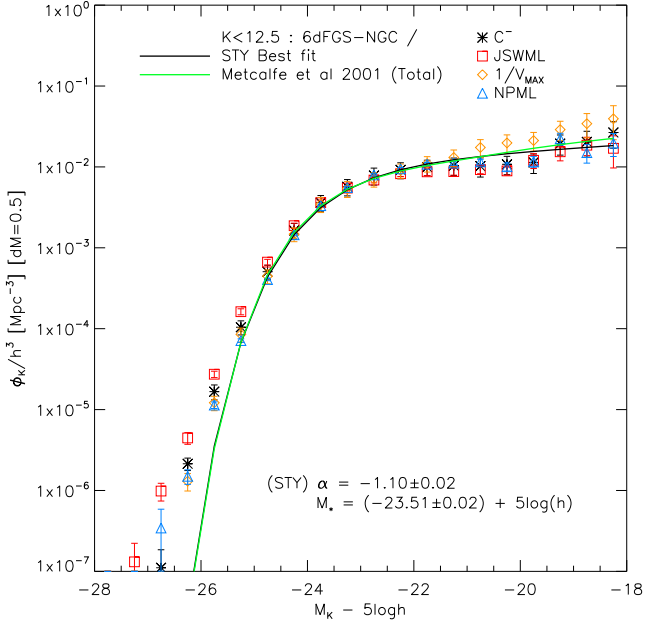


**Figure 4.** *K*-band galaxy LF estimates with  $7.5 < K < 12.5$  and  $dM = 0.5$  for the 6dFGS-NGC data. All of the estimates have been normalized using the  $n_1$  number density estimator for their respective LF.

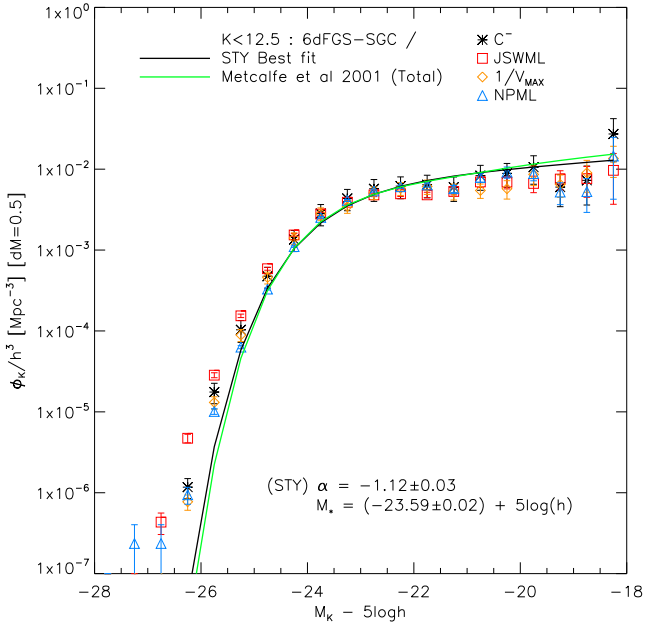


**Figure 5.** *K*-band galaxy LF estimates with  $7.5 < K < 12.5$  and  $dM = 0.5$  for the 6dFGS-SGC data. All of the estimates have been normalized using the  $n_1$  number density estimator for their respective LF.

between the Metcalfe et al. LF and the LF estimates we have made here.

In Fig. 8 we show the number density profile for the 6dFGS-SGC field. We again see good agreement between the different estimators of the density profile. However, at high redshift ( $z > 0.05$ ) the NPML estimate is significantly higher than the JSWML and  $C^-$  estimates. This is true for all three *K*-band fields and may therefore be indicative of a lack of robustness at high redshift for the NPML estimate. All profile estimates are particularly underdense at local redshift with the JSWML and  $C^-$  becoming homogeneous at deeper

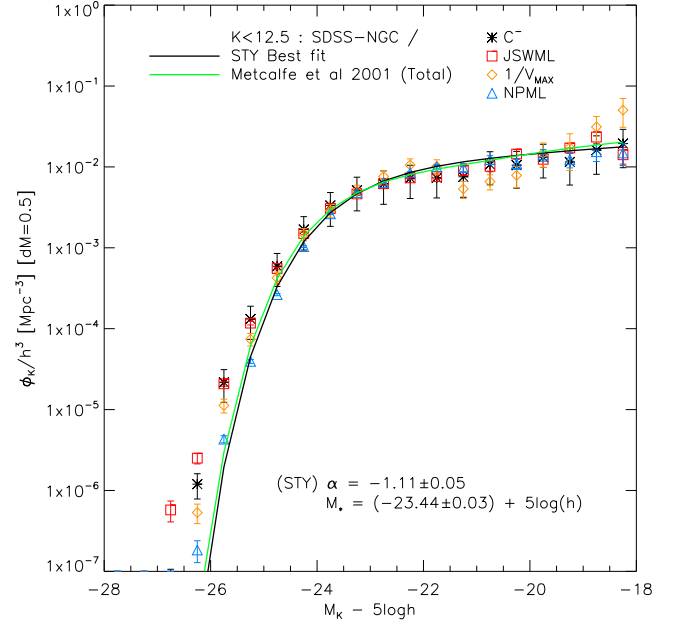


**Figure 6.** *K*-band galaxy LF estimates with  $7.5 < K < 12.5$  and  $dM = 0.5$  for the SDSS-NGC data. All of the estimates have been normalized using the  $n_1$  number density estimator for their respective LF.

redshifts. We again note the agreement with the Paper I (fig. 3b) number density profile for this field which once more reflects the validity of the Metcalfe et al. LF for the sample in this field.

Finally, in Fig. 9 we show the number density profile for the SDSS-NGC region. Here we see a similar pattern of agreement between the different number density profiles. The JSWML, NPML and  $C^-$  profiles are in agreement at low redshift in showing an underdense profiles with significant LSS (which we attribute to Coma at  $z = 0.023$ ). At deeper redshifts ( $z > 0.08$ ), the density profiles show evidence of an extensive overdensity. We return to investigate this issue using the deeper *r*-band data over the same field. However, we also note that this substantially inhomogeneous profile is in agreement with the density profile estimated in Paper I (fig. 3c).

We have evaluated the corresponding number underdensity indicated by these profiles as

$$\frac{\int_0^{z_1} \frac{n(z)}{n_K} \frac{dV}{dz} dz}{\int_0^{z_1} dV}. \quad (13)$$

The average of the profile number underdensities are reported in Table 1 for  $z < 0.05$ , i.e.  $\approx 150 h^{-1}$  Mpc, and  $z < 0.1$ , i.e.  $\approx 300 h^{-1}$  Mpc in the 6dFGS-NGC, 6dFGS-SGC and SDSS-NGC regions. Errors have been inferred using jackknife estimates. We noted earlier the potential lack of robustness at high redshift for the NPML estimator. We have therefore disregarded the NPML profiles in calculating the  $z < 0.1$  average underdensities.

These results are broadly consistent with the underdensities reported in Paper I (table 4) – aside from the 6dFGS-SGC estimate. In this case, both the  $z < 0.05$  (now  $0.76 \pm 0.05$ , previously  $0.60 \pm 0.05$ ) and  $z < 0.1$  results (now  $1.02 \pm 0.11$ , previously  $0.75 \pm 0.04$ ) are less underdense. Indeed the  $z < 0.1$  result is now consistent with homogeneity, albeit with larger errors. However, this difference is relatively minor in that the results presented here based on number count normalized number density profiles are in agreement with the 6dFGS-SGC number count underdensity reported in Paper I ( $0.76 \pm 0.03$ ).

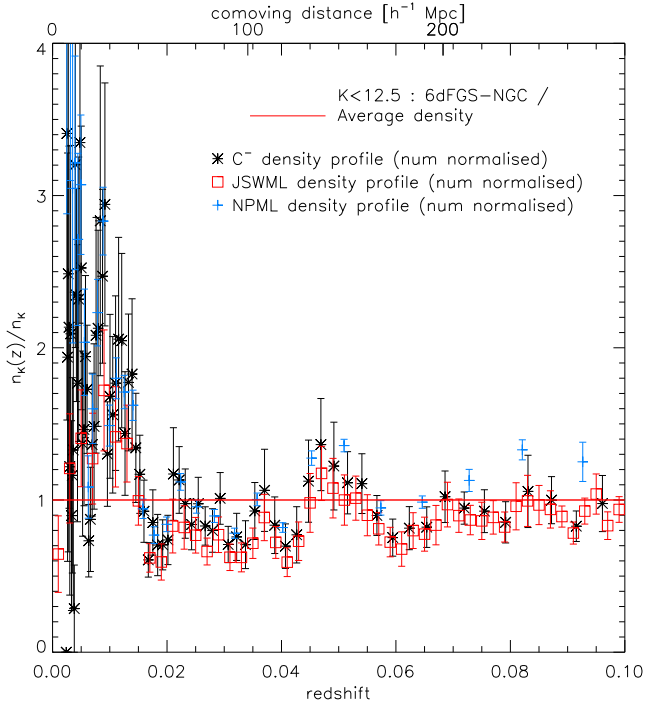


**Figure 7.** *K*-band galaxy number underdensity profile with  $7.5 < K < 12.5$  for the 6dFGS-NGC data normalized (for each LF) to the number counts in the region. The red (solid) line represents the homogeneous prediction for each LF.

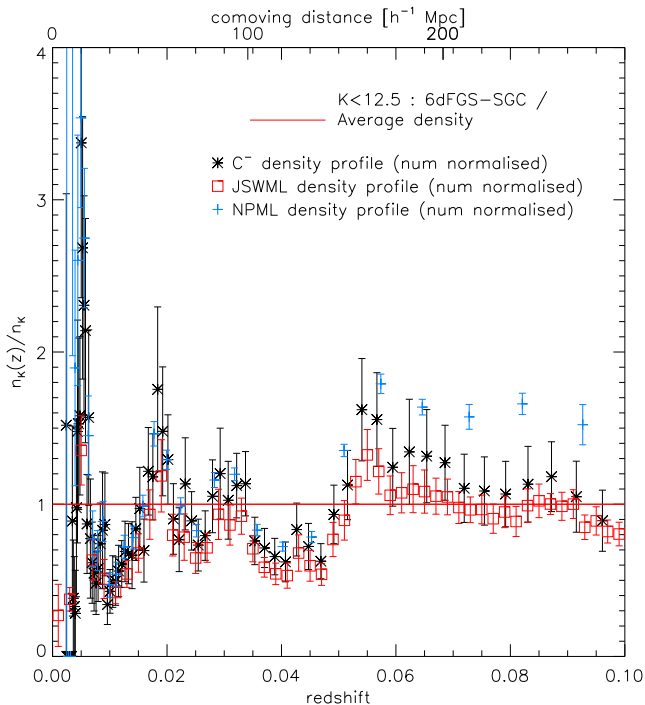


**Figure 8.** *K*-band galaxy number underdensity profile with  $7.5 < K < 12.5$  for the 6dFGS-SGC data normalized (for each LF) to the number counts in the region. The red (solid) line represents the homogeneous prediction for each LF.

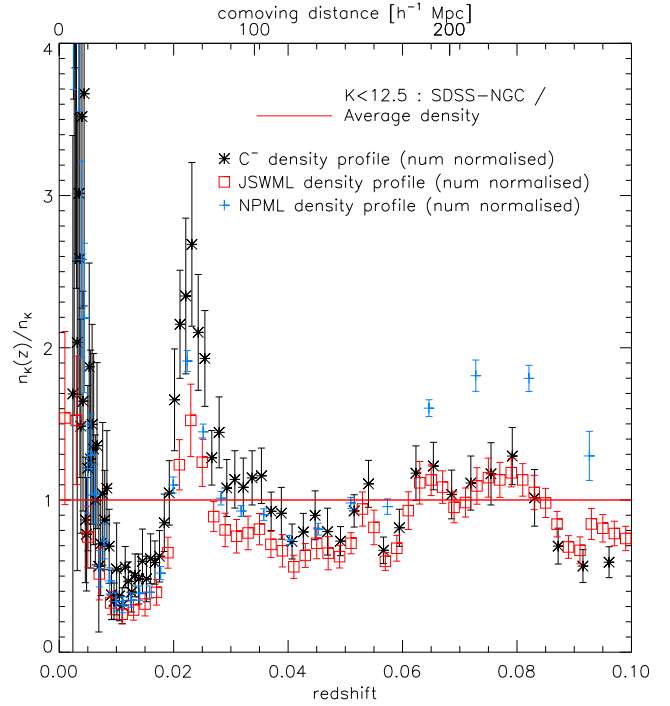


**Figure 9.** *K*-band galaxy number underdensity profile with  $7.5 < K < 12.5$  for the SDSS-NGC data normalized (for each LF) to the number counts in the region. The red (solid) line represents the homogeneous prediction for each LF.

**Table 1.** A summary of the average underdensities derived using equation (13). The  $z < 0.05$  and  $z < 0.1$  entries assume  $7.5 < K < 12.5$ .

Field	Sample limit	Underdensity
6dFGS-NGC	$z < 0.05$	$0.95 \pm 0.11$
6dFGS-SGC	$z < 0.05$	$0.76 \pm 0.05$
SDSS-NGC	$z < 0.05$	$0.83 \pm 0.05$
6dFGS-NGC	$z < 0.1$	$0.91 \pm 0.08$
6dFGS-SGC	$z < 0.1$	$1.02 \pm 0.11$
SDSS-NGC	$z < 0.1$	$0.89 \pm 0.06$

We therefore conclude that the density profiles show evidence for an LSS local underdensity for  $z < 0.05$  which the SDSS-NGC field in particular suggests may extend to deeper depths ( $\approx 300 h^{-1}$  Mpc). These conclusions are in agreement with those presented in [Paper I](#) which reflects the agreement found here with the Metcalfe et al. LF which was assumed in that study.

## 6 $r \leq 17$ LF AND DENSITY PROFILES IN THE SDSS-NGC REGION

Using the SDSS survey it is possible to go to deeper survey limits than in the *K* band. In particular, following [Paper I](#), we use an *r*-band limited sample in order to investigate the SDSS-NGC field. We have used a more conservative *r*-band magnitude limit of  $r \leq 17$  than the  $r \leq 17.2$  limit used in [Paper I](#) in order to minimize any potential biasing/issues associated with spectroscopic incompleteness.

Now in [Fig. 10](#) we show the  $V/V_{\max}$  estimates. We report a mean value of  $(0.500 \pm 0.003)$ . This value is consistent with the homogeneous expectation and indeed the uniformity in this statistic shows



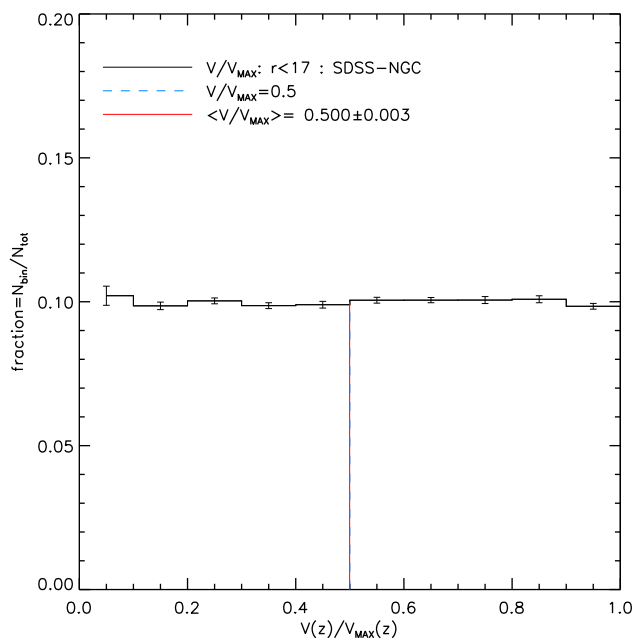


**Figure 10.** A histogram of  $r$ -band galaxy  $V/V_{\max}$  with  $10 < r < 17$  for the SDSS-NGC data with a corresponding jackknife error. The blue (dashed) line shows the homogeneous, complete expectation that  $\langle V/V_{\max} \rangle = 0.5$ . Also shown is the mean  $\langle V/V_{\max} \rangle$  for SDSS-NGC data (red, solid line).

little evidence for an underdensity. This is significantly different from the slope observed in Fig. 3 where the  $K$ -band SDSS-NGC  $V/V_{\max}$  estimates are shown. A similar and related situation was encountered in Paper I when comparing the results for the  $r$ - and  $K$ -band counts over the same field. Here it was concluded that the evidence for an underdensity in the  $r$ -band was more ambiguous and more suggestive of  $150 h^{-1}$  scale underdensity which was punctuated by the strong clustering associated with the Coma supercluster. This is potentially consistent with the broader smoothing effect of the  $d(V/V_{\max}) = 0.1$  binning used for the deeper  $r$ -band sample which may smooth over local variations in the density profile. We therefore proceed to investigate  $r$ -band LFs and the resulting density profiles.

In Fig. 11 we show the LF estimates for the SDSS-NGC region  $r$ -band data. We see that there is good agreement between the variety of LF estimates except for the very brightest objects ( $< M_* - 3$ ). We also note that the  $C^-$  estimator has a shallower faint end slope than compared to our other LF estimators. However, again, these differences are relatively minor in that the Metcalfe et al. LF is a good representation of our results over a wide range of magnitudes.

We therefore show in Fig. 12 the density profiles associated with JSWML,  $C^-$  and NPML LF estimates  $r$ -band SDSS-NGC density profiles. The JSWML,  $C^-$  and NPML profiles are in good agreement in showing underdense profiles with significant LSS (which we attribute to Coma at  $z = 0.023$ ). At deeper redshifts ( $z > 0.08$ ) the  $C^-$ , NPML and JSWML density profiles remain significantly inhomogeneous. This is consistent with the investigation of fainter GAMA  $K$ -band and SDSS  $r$ -band  $n(m)$  and  $n(z)$  in Paper I which indicated that an inhomogeneity could extend beyond  $z = 0.1$  in the SDSS-NGC region. We also note that the  $r$ -band density profiles demonstrate a similar local underdensity ( $z < 0.08$ ) to that seen over the same field in the  $K$  band (see Fig. 9).

Finally, we have evaluated the average number underdensity following equation (13) with the results shown in Table 2. We now include the NPML density profiles for the  $z < 0.1$  results as there is no evidence of lack of robustness at high redshift for the  $r$ -band

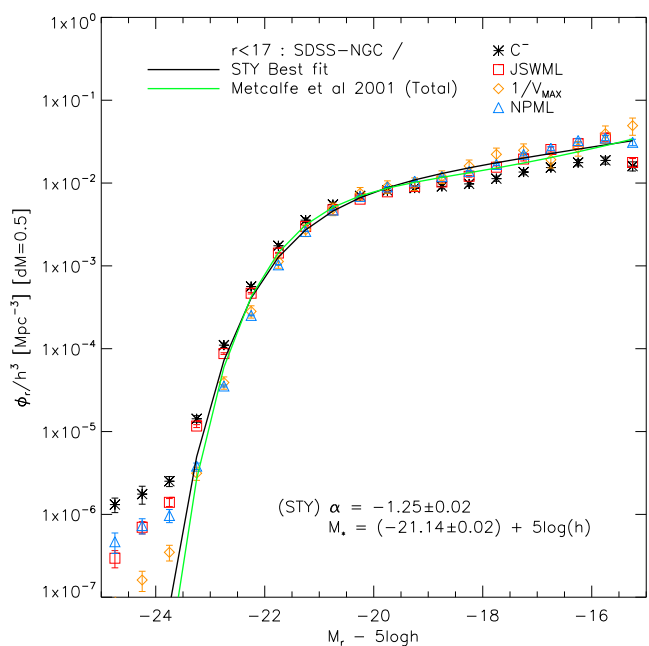


**Figure 11.**  $r$ -band galaxy LF estimates with  $10 < r < 17$  and  $dM = 0.5$  for the SDSS-NGC data. All of the estimates have been normalized using the  $n_1$  number density estimator for their respective LF.

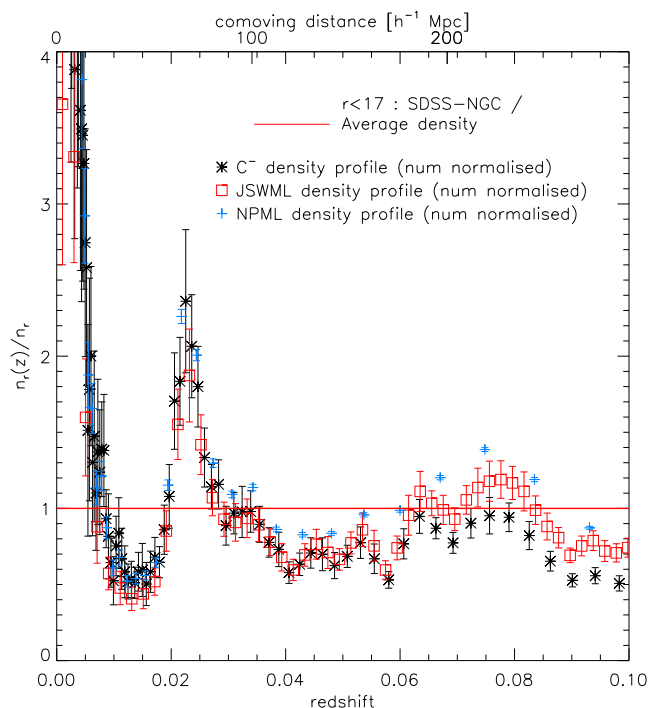


**Figure 12.**  $r$ -band galaxy number density profile with  $10 < r < 17$  for the SDSS-NGC data normalized (for each LF) to the number counts in the region. The red (solid) line represents the homogeneous prediction for each LF.

**Table 2.** A summary of the average underdensities derived using equation (13). The  $z < 0.05$  and  $z < 0.1$  entries assume  $10 < r < 17$ .

Field	Sample limit	Underdensity
SDSS-NGC	$z < 0.05$	$0.83 \pm 0.05$
SDSS-NGC	$z < 0.10$	$0.90 \pm 0.03$

sample. For  $z < 0.05$  we find an average number underdensity of  $[0.83 \pm 0.05]$  which is in agreement with the  $K$ -band SDSS-NGC results in suggesting a significant local number underdensity ( $\approx 150 h^{-1}$  Mpc). Whilst the  $z < 0.1$  average number underdensity of  $[0.90 \pm 0.03]$  indicates a more extensive inhomogeneity on  $\approx 300 h^{-1}$  Mpc scales. Both these results are in agreement with the results presented in [Paper I](#).

We conclude that the  $r$ -band density profiles show evidence for an underdensity, which is punctuated by the Coma cluster producing a strong overdensity. This underdensity is similar to those observed for the corresponding region in the  $K$  band (Fig. 9) but less than that observed in the  $K$  band over the SGC (Fig. 8).

## 7 DISCUSSION

We note that any estimation of the LF is strongly dependent on accurate and stable galaxy photometry. [Paper I](#) includes a fuller discussion of the photometric completeness of these samples. However, we have estimated the effect of magnitude errors on our NIR LF estimation using the method of Efstathiou et al. (1988) where the observed LF is described as the convolution of the true underlying LF with a magnitude error kernel, i.e.  $\phi_{\text{obs}}(M) = g(M) \otimes \phi_{\text{true}}(M)$ . Using realistic magnitude error kernels derived from fig. A1 of [Paper I](#) we find that the effects of magnitude errors on the  $K$ -band LF typically steepen the faint end slope by  $\approx 0.1$  and similarly brighten the characteristic magnitude by  $\approx 0.1$ . We have investigated the uncertainty this corresponds to in our determination of the galaxy number density profiles by testing the variation induced in the Cole (2011) density profiles if a realistic magnitude error is allowed. We found that the changes were small, typically  $< 1\text{--}2$  per cent ( $K$ - and  $r$ -band, respectively) and random in nature. It should be noted that larger ( $\approx 5$  per cent) variations were possible for low and high  $z$  ( $z < 0.01$  and  $z > 0.1$ ). However, over the redshift range of interest we conclude that magnitude errors only weakly affect our density profile estimates.

We again follow [Paper I](#) in the treatment of completeness issues. We note that the inclusion of corrections for incompleteness detailed for the  $V_{\text{max}}$ ,  $C^-$  and STY methods are relatively minor in determining the LF or number density profiles. Finally, we also again note that we have used the  $vc$  2MASS quality flag to reject artefact and non-extragalactic objects. This ensures that  $\approx 100$  per cent of objects  $7.5 < K < 12.5$  have been visually inspected to ensure a high purity sample.

An important assumption in this work has been the use of the  $K + E$  prescriptions used in Metcalfe et al. (2001, 2006). In order to explain the observed underdensity we would require evolutionary brightening at  $z \approx 0.1$  or a more negative  $K$ -correction. As was noted in [Paper I](#) an argument against the rise in number density being caused by  $z \approx 0.1$  galaxy evolution is the rise in number counts across the NIR and optical bands ( $B, R, I, H, K$ ) – Metcalfe et al. (2001, 2006). A local underdensity produces just this, an approximately band-independent rise in the bright number counts whereas evolutionary effects correspond to a greater effect in the bluer bands and at fainter magnitudes. We also note that in [Paper I](#) we investigated alternative evolutionary models as well as no evolutionary corrections and found minimal differences in the  $K$  band (although not for the  $r$  band) in terms of derived redshift distributions and number counts.

The three fields studied here are wide field, with each representing  $\approx 1/15$  of the sky. However, they are considerably smaller than the full sky 2MASS sample from which they are drawn. We note however that Appleby & Shafieloo (2014) have investi-

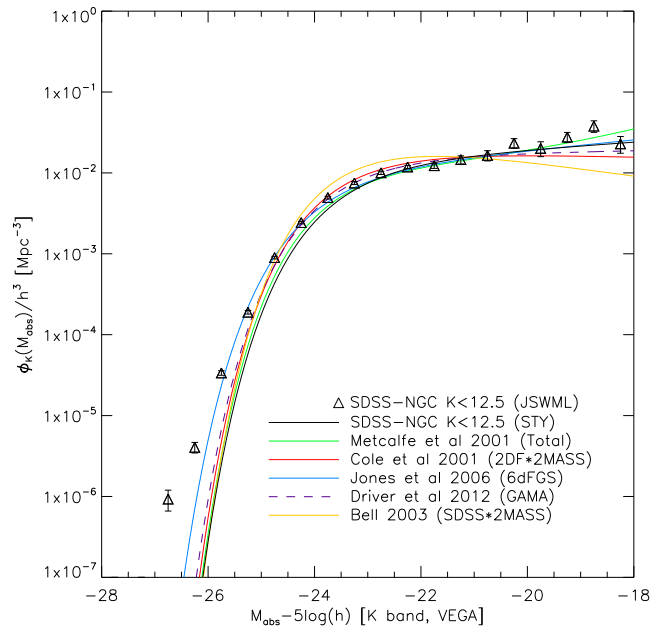


**Figure 13.** A comparison of various parametric  $K$ -band LF estimates using the full  $\phi_K(M)$ . Results have been normalized to a common and arbitrary number density estimated using the Metcalfe et al. LF over the range  $-28 \leq M - 5 \log(h) \leq -18$ . Parameters taken from Cole et al. (2001), Jones et al. (2006), Driver et al. (2012) and Bell et al. (2003).

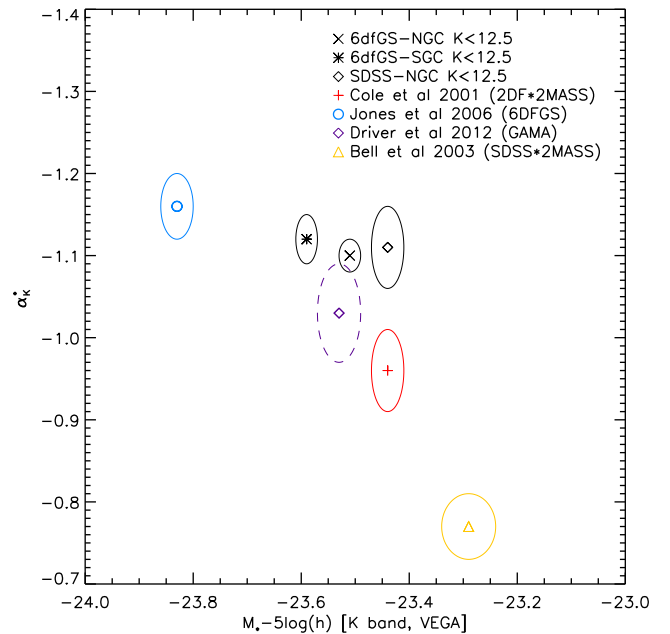


**Figure 14.** A comparison of various  $K$ -band parametric LF estimates of the Schechter  $\alpha$  and  $M_*$  parameters. We have not been able to represent the covariance between  $\alpha$  and  $M_*$  from the studies shown so we assume no covariance.

gated the isotropy of LF shape estimates using the 2MPZ, a set of photometric redshifts estimated in Bilicki et al. (2014) for the 2MASS-XSC sample. These authors find no significant evidence for anisotropy in non-parametric LF shape estimates. This suggests that the three fields used in this study should be representative of the full 2MASS survey. It should be noted that the LF normalization was not

investigated in this paper so this result is not in tension with the varying galaxy number density profiles presented in this study. Furthermore, it is also of interest that these authors report weak evidence for a dipole asymmetry in parametric LF estimates between the north and south galactic plane. This is again in agreement with the significantly different density profiles found for the 6DFGS-SGC, 6DFGS-NGC and SDSS-NGC regions.

Other estimates of the NIR LF using these samples have been attempted. We therefore now present in Figs 13 and 14 a comparison to other studies' estimates of the Schechter  $\alpha$  and  $M_*$  parameters. In Fig. 13 we show a comparison of the full  $\phi(M)$  because it captures the correlation between the  $\alpha$  and  $M_*$  parameters. We also include in this comparison our JSWML non-parametric LF estimates (SDSS-NGC) so that any deviations from the Schechter form can be judged. After normalizing to a common and arbitrary number density [estimated using the Metcalfe et al. LF over the range  $-28 \leq M - 5 \log(h) \leq -18$ ], we find that the  $K$ -band LF estimates are relatively consistent, except at the faint end where there is greater variance. In particular, the Metcalfe et al. LF shows a much steeper faint-end slope than found by Bell et al. (2003) using the  $V_{\max}$  estimator with the 2MASS survey. We attribute this to photometric problems in the early 2MASS data releases since in the same work the  $g$ -band selected NIR LF was estimated to have a faint end slope of  $\alpha = -1.33$  which is in rough agreement with the steeper slope of the Metcalfe et al. LF.

In Fig. 14 most  $K$ -band LF parametrizations occupy the usual degenerate strip between  $M^*$  and  $\alpha$ . The one that most deviates from this line is the LF of Jones et al. (2006) (see also Fig. 13). We also note that the variation between different LF estimates is much larger than would be expected on the basis of the 'naive' error ellipses (i.e. the no covariance case). We do not understand what causes these differences but potential causes of differences are different treatment of flow models, incompleteness, as well as real differences in sample selection (magnitude limits, redshift ranges, etc.).

We have made a similar comparison for  $r$ -band LF estimates in Figs 15 and 16. We have again normalized to an arbitrary number density estimated using the Metcalfe et al. LF over the range  $-25 \leq M - 5 \log(h) \leq -15$ . Results quoted in the  $r_{0.1}$  band (i.e. corrected to a  $z = 0.1$  rest frame as per Blanton et al. 2003) have been converted into the  $r$  band as  $r_{0.1} \approx r + 0.23$  (Nichol et al. 2006). We find results that are consistent with the Metcalfe et al. LF. However, the Blanton et al. (2003) and Driver et al. (2012) estimates show a significantly sharper bright end fall off and a shallower faint end slope than the Metcalfe et al. LF. The greater uncertainties in the assumed evolutionary model for the  $r$  band as compared to the  $K$  may explain the difference with the Driver et al. (2012) LF since the GAMA survey probes a substantially deeper redshift range than the samples used in this paper. However, this is an unlikely explanation for the difference with the SDSS-based Blanton et al. (2003) LF, especially as any evolutionary modelling effects would be expected to primarily affect  $M_*$  estimates. It is therefore unclear why these results are different from those presented here. However, we agree with the observation of Montero-Dorta & Prada (2009) that the size of the SDSS sample has increased considerably since the pre SDSS-DR1 results used in Blanton et al. (2003). The resulting improvements in magnitude limits may have resulted in substantial improvements in sample selection. The potential uncertainty that differences in the LF correspond to in the number density profiles is indicated by the differences between the  $C^-$ , JSWML and NPML density profiles in Fig. 12. This is particularly relevant in the case of the  $C^-$  LF estimate where we find a flatter faint end slope than

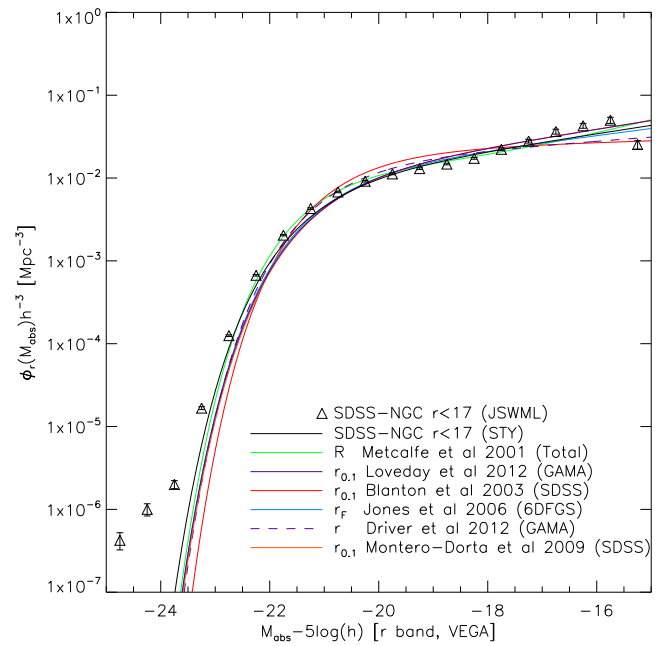


**Figure 15.** A comparison of various  $r$ -band LF estimates using the full  $\phi_r(M)$ . Results have been normalized to a common and arbitrary number density estimated using the Metcalfe et al. LF over the range  $-25 \leq M - 5 \log(h) \leq -15$ . Parameters taken from Loveday et al. (2012), Jones et al. (2006), Blanton et al. (2003), Driver et al. (2012) and Montero-Dorta & Prada (2009). Results quoted in the  $r_{0.1}$  band have been converted into the  $r$  band as  $r_{0.1} \approx r + 0.23$  (Nichol et al. 2006).

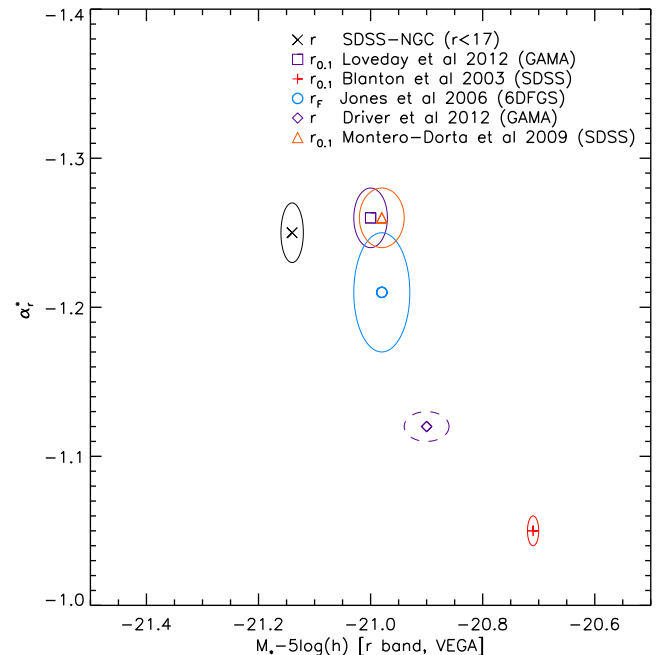


**Figure 16.** A comparison of various  $r$ -band parametric LF estimates of the Schechter  $\alpha$  and  $M_*$  parameters. We have not been able to represent the covariance between  $\alpha$  and  $M_*$  from the studies shown so we assume no covariance. Again, results quoted in the  $r_{0.1}$  band have been converted into the  $r$  band as  $r_{0.1} \approx r + 0.23$  (Nichol et al. 2006).

the JSWML or NPML estimates (see Fig. 11) but nevertheless find similar number density profiles.

Again many,  $r$ -band LF parametrizations occupy the usual degenerate strip between  $M^*$  and  $\alpha$  in Fig. 16. The two that most deviate from this line are the LFs of Loveday et al. (2012) and Montero-Dorta & Prada (2009, see also Fig. 15). However, this small deviation may be attributable to the correction applied to convert from the  $r_{0.1}$  and  $r$  bands. Fig. 16 also confirms the much flatter parametric faint end slope reported by Blanton et al. (2003) than seen by later authors, including ourselves.

## 8 CONCLUSIONS

We have used samples from 6dFGS/2MASS and SDSS to simultaneously investigate the local LF and galaxy number density profiles. We have studied three large volumes which cover much of the sky and find evidence for an anisotropic galaxy distribution. In particular we observe a local number underdensity out to  $\approx 150 h^{-1}$  Mpc around our position in the SGC which both the  $r$  and  $K$  band SDSS-NGC samples suggest may extend deeper to  $\approx 300 h^{-1}$  Mpc. We have also found evidence that the Metcalfe et al. LF assumed in Paper I is an adequate fit for these samples and hence the density profiles presented there may be unbiased by this choice. This work also complements previous studies which have investigated variation of luminosity density with redshift (Keenan et al. 2012, 2013) by providing estimates of variation in number density. The estimate made in Paper I of an  $\approx 15$  per cent number underdensity is broadly consistent with the Keenan et al. (2013) estimate of an  $\approx 50$  per cent increase in luminosity between the local universe and  $z \approx 0.1$ .

A significant advantage of investigating both the  $K$  and  $r$  bands is that an underdensity might be indicated if the effect is band independent, although a band-dependent result might still be explained by different galaxy clustering bias applying in the different bands. We note that the  $r$ -band SDSS-NGC profile (Fig. 12) shows a similar underdensity to the corresponding  $K$ -band estimate (Fig. 9) with only small differences at low redshift. But both are in agreement in supporting an underdensity continuing beyond  $z \approx 0.1$ . One important route for continuing the investigation into the isotropy of the galaxy distribution will be the incorporation of peculiar velocity fields. We therefore believe that the ongoing investigation into the 6dFGS peculiar velocity field as determined using the Fundamental Plane (and its comparison to that inferred from PSCz) started in Springob et al. (2014) will be of particular interest. We note that the initial analysis presented in Springob et al. (2014) is in agreement with the PSCz estimated density field (to a separately estimated 2MRS peculiar velocity field based on an update of Erdoğan et al. 2006) which has a mean underdensity of 11 per cent within  $180 h^{-1}$  Mpc. The density profiles presented here are consistent with such a local underdensity.

## ACKNOWLEDGEMENTS

We thank Richard Fong, John Lucey, Alan Heavens and Ryan Keenan for useful comments. JRW acknowledges financial support from STFC. We would also like to thank the anonymous referee for their comments.

We acknowledge the use of a modified version of the JSWML code accompanying Cole (2011).

This research has made use of the NASA/IPAC Extragalactic Database (NED) which is operated by the Jet Propulsion Laboratory, California Institute of Technology, under contract with the National Aeronautics and Space Administration.

We would also like to acknowledge the use of the TOPCAT utility (Taylor 2005).

This research has made use of the VizieR catalogue access tool, CDS, Strasbourg, France. The original description of the VizieR service was published in A&AS 143, 23 (2000).

Funding for the SDSS and SDSS-II has been provided by the Alfred P. Sloan Foundation, the Participating Institutions, the National Science Foundation, the US Department of Energy, the National Aeronautics and Space Administration, the Japanese Monbukagakusho, the Max Planck Society, and the Higher Education Funding Council for England. The SDSS web site is <http://www.sdss.org/>.

The SDSS is managed by the Astrophysical Research Consortium for the Participating Institutions. The Participating Institutions are the American Museum of Natural History, Astrophysical Institute Potsdam, University of Basel, University of Cambridge, Case Western Reserve University, University of Chicago, Drexel University, Fermilab, the Institute for Advanced Study, the Japan Participation Group, Johns Hopkins University, the Joint Institute for Nuclear Astrophysics, the Kavli Institute for Particle Astrophysics and Cosmology, the Korean Scientist Group, the Chinese Academy of Sciences (LAMOST), Los Alamos National Laboratory, the Max-Planck-Institute for Astronomy (MPIA), the Max-Planck-Institute for Astrophysics (MPA), New Mexico State University, Ohio State University, University of Pittsburgh, University of Portsmouth, Princeton University, the United States Naval Observatory, and the University of Washington.

This publication makes use of data products from the Two Micron All Sky Survey, which is a joint project of the University of Massachusetts and the Infrared Processing and Analysis Center/California Institute of Technology, funded by the National Aeronautics and Space Administration and the National Science Foundation.

## REFERENCES

- Appleby S., Shafieloo A., 2014, *J. Cosmol. Astropart. Phys.*, 10, 70
- Bell E. F., McIntosh D. H., Katz N., Weinberg M. D., 2003, *ApJS*, 149, 289
- Bilicki M., Jarrett T. H., Peacock J. A., Cluver M. E., Steward L., 2014, *ApJS*, 210, 9
- Blanton M. R. et al., 2003, *ApJ*, 592, 819
- Böhringer H., Chon G., Bristow M., Collins C. A., 2015, *A&A*, 574, A26
- Bruzual G., Charlot S., 2003, *MNRAS*, 344, 1000
- Busswell G. S., Shanks T., Frith W. J., Outram P. J., Metcalfe N., Fong R., 2004, *MNRAS*, 354, 991
- Carroll S. M., 2001, *Living Rev. Relativ.*, 4, 1
- Choloniewski J., 1986, *MNRAS*, 223, 1
- Choloniewski J., 1987, *MNRAS*, 226, 273
- Clarkson C., Maartens R., 2010, *Class. Quantum Gravity*, 27, 124008
- Cole S., 2011, *MNRAS*, 416, 739
- Cole S. et al., 2001, *MNRAS*, 326, 255
- Colin J., Mohayaee R., Sarkar S., Shafieloo A., 2011, *MNRAS*, 414, 264
- Conley A., Carlberg R. G., Guy J., Howell D. A., Jha S., Riess A. G., Sullivan M., 2007, *ApJ*, 664, L13
- Davis M., Huchra J., 1982, *ApJ*, 254, 437
- de Lapparent V., Geller M. J., Huchra J. P., 1989, *ApJ*, 343, 1
- Driver S. P. et al., 2012, *MNRAS*, 427, 3244
- Efstathiou G., Ellis R. S., Peterson B. A., 1988, *MNRAS*, 232, 431
- Erdoğan P. et al., 2006, *MNRAS*, 373, 45
- Feindt U. et al., 2013, *A&A*, 560, A90
- Felten J. E., 1976, *ApJ*, 207, 700
- Frith W. J., Busswell G. S., Fong R., Metcalfe N., Shanks T., 2003, *MNRAS*, 345, 1049

- Frith W. J., Outram P. J., Shanks T., 2005, in Fairall A. P., Woudt P. A., eds, ASP Conf. Ser. Vol. 329, *Nearby Large-Scale Structures and the Zone of Avoidance*. Astron. Soc. Pac., San Francisco, p. 49
- Frith W. J., Shanks T., Outram P. J., 2005, MNRAS, 361, 701
- Frith W. J., Outram P. J., Shanks T., 2006, MNRAS, 373, 759
- Ilbert O. et al., 2005, A&A, 439, 863
- Jarrett J. H., Chester T., Cutri R., Schneider S. E., Huchra J. P., 2003, AJ, 125, 525
- Jha S., Riess A. G., Kirshner R. P., 2007, ApJ, 659, 122
- Johnston R., 2011, A&AR, 19, 41
- Jones D. H., Peterson B. A., Colless M., Saunders W., 2006, MNRAS, 369, 25
- Jones D. H. et al., 2004, MNRAS, 355, 747
- Kafka P., 1967, Nature, 213, 346
- Keenan R. C., Trouille L., Barger A. J., Cowie L. L., Wang W., 2010, ApJS, 186, 94
- Keenan R. C., Barger A. J., Cowie L. L., Wang W.-H., Wold I., Trouille L., 2012, ApJ, 754, 131
- Keenan R. C., Barger A. J., Cowie L. L., 2013, ApJ, 775, 62
- Kraśniński A., 2014, Phys. Rev. D, 89, 023520
- Loveday J. et al., 2012, MNRAS, 420, 1239
- Lynden-Bell D., 1971, MNRAS, 155, 95
- Metcalfe N., Shanks T., Campos A., McCracken H. J., Fong R., 2001, MNRAS, 323, 795
- Metcalfe N., Shanks T., Weilbacher P. M., McCracken H. J., Fong R., Thompson D., 2006, MNRAS, 370, 1257
- Montero-Dorta A. D., Prada F., 2009, MNRAS, 399, 1106
- Nichol R. C. et al., 2006, MNRAS, 368, 1507
- Perlmutter S. et al., 1999, ApJ, 517, 565
- Planck Collaboration XVI, 2014, A&A, 571, A16
- Sandage A., Tammann G. A., Yahil A., 1979, ApJ, 232, 352
- Schechter P., 1976, ApJ, 203, 297
- Schmidt M., 1968, ApJ, 151, 393
- Schmidt B. P. et al., 1998, ApJ, 507, 46
- Schwarz D. J., 2012, *Cosmological backreaction*, The Twelfth Marcel Grossmann Meeting, p. 533
- Shanks T., 1990, in Bowyer S., Leinert C., eds, Proc. IAU Symp. 139, *The Galactic and Extragalactic Background Radiation*. Kluwer, Dordrecht, p. 269
- Soneira R. M., 1979, ApJ, 230, L63
- Springob C. M. et al., 2014, MNRAS, 445, 2677
- Takeuchi T. T., Yoshikawa K., Ishii T. T., 2000, ApJS, 129, 1
- Taylor M. B., 2005, in Shopbell P., Britton M., Ebert R., eds, ASP Conf. Ser. Vol. 347, *Astronomical Data Analysis Software and Systems XIV*. Astron. Soc. Pac., San Francisco, p. 29
- Whitbourn J. R., Shanks T., 2014, MNRAS, 437, 2146 (Paper I)
- Willmer C. N. A., 1997, AJ, 114, 898
- Wojtak R., Knebe A., Watson W. A., Iliev I. T., Heß S., Rapetti D., Yepes G., Gottlöber S., 2014, MNRAS, 438, 1805
- York D. G. et al., 2000, AJ, 120, 1579
- Zehavi I., Riess A. G., Kirshner R. P., Dekel A., 1998, ApJ, 503, 483
- Zucca E., Pozzetti L., Zamorani G., 1994, MNRAS, 269, 953
- Zucca E. et al., 1997, A&A, 326, 477

This paper has been typeset from a  $\text{\LaTeX}$  file prepared by the author.